Calponin-homology domain of GAS2L1 promotes formation of stress fibers and focal adhesions

Franco K.C. Au[a,#,†], Khoi T.D. Le[a,#], Zhitao Liao[b], Zhijie Lin[a,‡], Yuehong Shen[a,§], Penger Tong[b], Mingjie Zhang[a,‖], and Robert Z. Qi[a,c,*]

[a]Division of Life Science and State Key Laboratory of Molecular Neuroscience, The Hong Kong University of Science and Technology, Hong Kong, China; [b]Department of Physics, The Hong Kong University of Science and Technology, Hong Kong, China; [c]Bioscience and Biomedical Engineering Thrust, The Hong Kong University of Science and Technology (Guangzhou), Guangzhou 511453, China

ABSTRACT **Growth arrest–specific 2-like 1 protein (GAS2L1) binds both actin and microtubules through its unique structural domains: a calponin-homology (CH) domain for actin binding and a GAS2-related (GAR) domain for microtubule interaction. In this study, we demonstrate that GAS2L1 promotes stress fiber assembly, enhances focal adhesion formation, and stabilizes cytoskeletal networks against mechanical perturbation through its CH domain. Remarkably, we show that the CH domain dimerizes and induces actin filament bundling and stabilization both in cells and in vitro. The CH and GAR domains interact to form an autoinhibitory module, wherein the GAR domain suppresses CH domain dimerization and actin-bundling activity. Our findings provide novel insights into the regulatory mechanisms of GAS2L1's autoinhibition and identify the CH domain as a critical actin-bundling factor that contributes to the organization of stress fibers and focal adhesions.**

SIGNIFICANCE STATEMENT

- GAS2L1, containing a single CH domain, has been implicated in connecting F-actin and microtubules to centrioles before mitotic entry. However, the precise functional characteristics of GAS2L1's CH domain remain elusive.
- The authors demonstrated that GAS2L1 depletion hinders stress fiber and focal adhesion formation, whereas GAS2L1 or its CH domain overexpression exerts the opposite effect. The dimerization of GAS2L1's CH is required for cross-linking and bundling actin filaments. GAS2L1's GAR domain inhibits its CH dimerization, impeding the dimerization-mediated bundling of F-actin.
- The study demonstrates the multifaceted role of GAS2L1 in regulating focal adhesion dynamics via its single CH domain.

Monitoring Editor
Peter Bieling
Max Planck Institute of Molecular Physiology

Received: Oct 8, 2024
Revised: Jan 27, 2025
Accepted: Feb 12, 2025

INTRODUCTION

In eukaryotic cells, the actin cytoskeleton is a dynamic structure that constantly remodels itself in response to various cellular signals. Actin exists in two forms: globular monomeric actin (G-actin) and filamentous polymeric actin (F-actin). F-actin often organizes into higher-order structures such as filopodia, lamellipodia, and stress fibers, which are essential for a variety of cellular functions, including shape maintenance, adhesion, and migration. These structures are continually remodeled by the exchange of actin subunits and actin-binding proteins (ABPs) between the cytoskeleton and the cytoplasm (Pollard and Cooper, 1986; dos Remedios *et al.*, 2003; Carlsson, 2010; Kadzik *et al.*, 2020).

Stress fibers, composed of bundled F-actin, play a pivotal role in regulating cell spreading, shape maintenance, and the formation of focal adhesions (Tojkander *et al.*, 2012; Skau and Waterman, 2015). Focal adhesions are dynamic structures that anchor cells to the extracellular matrix and serve as sites of mechanical signaling and force transduction (Gardel *et al.*, 2010; Parsons *et al.*, 2010). The assembly of focal adhesions begins with the formation of small, nascent focal complexes in the lamellipodia, which rely on actin polymerization (Zaidel-Bar *et al.*, 2003; Choi *et al.*, 2008). While many focal complexes disassemble shortly after formation, a subset mature into larger focal adhesions through the action of myosin II, which generates contractile forces that promote stress fiber assembly (Chrzanowska-Wodnicka and Burridge, 1996; Riveline *et al.*, 2001; Peterson *et al.*, 2004; Hotulainen and Lappalainen, 2006; Vicente-Manzanares *et al.*, 2007). These stress fibers further recruit additional focal adhesion proteins, facilitating the maturation process (Oakes *et al.*, 2012). Once mature, focal adhesions serve as stable anchorage points, transmitting traction forces from the actomyosin cytoskeleton and mediating mechanical signaling and cell migration (Gardel *et al.*, 2010; Geiger and Yamada, 2011).

The assembly and regulation of the actin cytoskeleton are coordinated by various ABPs, some of which contain a conserved calponin-homology (CH) domain—a known F-actin–binding motif. The CH domain was originally identified in the N-terminus of calponin and has since been classified into three types: CH1 and CH2, which typically appear as a tandem pair, and CH3, which exists independently as a single CH domain (Bañuelos *et al.*, 1998; Gimona *et al.*, 2002; Korenbaum and Rivero, 2002; Yin *et al.*, 2020). The CH1-CH2 tandem functions as a complete F-actin–binding module and is found in classical ABPs like α-actinin, filamin, and β-spectrin, where CH1 confers F-actin–binding activity while CH2 alone is inactive (Gimona *et al.*, 2002; Yin *et al.*, 2020). When combined, the CH1-CH2 tandem binds F-actin more strongly than CH1 alone. CH3, on the other hand, is present in proteins with diverse functions, some of which lack F-actin–binding activity (Gimona *et al.*, 2002).

The growth arrest–specific 2 (GAS2) family of proteins is a unique subset of CH-containing proteins that bind both F-actin and microtubules (Gimona *et al.*, 2002; Korenbaum and Rivero, 2002; Goriounov *et al.*, 2003). In mammals, the GAS2 family comprises at least four members: GAS2, GAS2-like 1 (GAS2L1), GAS2-like 2 (GAS2L2), and GAS2-like 3 (GAS2L3), all of which contain an N-terminal CH domain (CH3), followed by a GAS2-related (GAR) domain for microtubule binding (Schneider *et al.*, 1988; Goriounov *et al.*, 2003; Stroud *et al.*, 2011, 2014). While GAS2 has a minimal C-terminal region following the GAR domain, the GAS2-like proteins possess a larger C-terminal region that includes a Ser-x-Ile-Pro (SxIP) motif, which binds end-binding proteins to track microtubule plus-ends (Jiang *et al.*, 2012; Stroud *et al.*, 2014). Among these family members, GAS2L1 has been implicated in several cellular processes, including centrosome disjunction before mitotic entry through the tethering of F-actin and microtubules to centrioles (Au *et al.*, 2017, 2020). Furthermore, GAS2L1 plays a role in promoting axon outgrowth and branching in neurons and contributes to sperm motility and the organization of axonemal structures (Gamper *et al.*, 2016; van de Willige *et al.*, 2019).

To further investigate the functional roles of GAS2L1, we examined the effects of *gas2l1* knockout on cellular phenotypes. Our results show that GAS2L1 removal impairs the formation of stress fibers and focal adhesions, while overexpression of GAS2L1 or its CH domain enhances the assembly of these structures. Mechanistically, we found that the CH domain of GAS2L1 forms a dimer that cross-links and bundles actin filaments, thereby stabilizing them. This dimerization is inhibited by the binding of the GAR domain to the CH domain, which prevents the dimerization-mediated bundling of F-actin. Thus, we propose that the regulation of CH dimerization by the GAR domain represents a unique mechanism controlling GAS2L1's actin-binding and -bundling activity.

RESULTS

GAS2L1 functions in the formation of actin stress fibers and focal adhesions

To investigate the role of GAS2L1 in actin organization, we previously generated *gas2l1*$^{-/-}$ RPE-1 cells using the CRISPR/Cas9 system (Au *et al.*, 2020). In this study, we visualized actin filaments in both parental and *gas2l1*$^{-/-}$ RPE-1 cells by staining with fluorescent dye-conjugated phalloidin. While the actin staining patterns at the cell periphery appeared similar in both cell types, *gas2l1*$^{-/-}$ cells displayed a marked reduction in the average intensity (~53%) and number (~43%) of individual stress fibers compared with the parental cells (Figure 1A). Re-expression of GAS2L1 in the knockout cells effectively restored both the intensity and number of stress fibers (Figure 1A).

This article was published online ahead of print in MBoC in Press (http://www.molbiolcell.org/cgi/doi/10.1091/mbc.E24-10-0444) on February 19, 2025.

[#]These authors contributed equally to this work.

Author contributions: R.Z.Q. and F.K.C.A. conceived and designed the experiments; R.Z.Q. and F.K.C.A. drafted the article; F.K.C.A., K.T.D.L., and Z.L. performed the experiments; F.K.C.A., K.T.D.L., and Z.L. analyzed the data; F.K.C.A., K.T.D.L., and Z.L. prepared the digital images; Y.S. reviewed and edited the manuscript; P.T. and M.Z. reviewed, edited the manuscript, and acquired funding.

Conflict of interest: The authors declare no competing financial interests.

Present addresses: [†]Department of Cellular and Molecular Medicine, University of California at San Diego, La Jolla, CA; [‡]Zhejiang Key Laboratory of Organ Development and Regeneration, College of Life and Environmental Sciences, Hangzhou Normal University, Hangzhou, China; [§]Department of Oral and Maxillofacial Surgery, Stomatological Center, Peking University Shenzhen Hospital, Shenzhen, China; [‖]School of Life Sciences, Southern University of Science and Technology, Shenzhen, China.

*Address correspondence to: Robert Z. Qi (qirz@ust.hk).

Abbreviations used: ABP, actin-binding proteins; ABS, actin-binding site; AFM, atomic force microscopy; BS^3, bi(sulfosuccinimidyl)suberate; CH, calponin-homology; GAR, GAS2-related; GAS2L1, growth arrest-specific 2-like 1; SPTB2, spectrin βII; SxIP, Ser-x-Ile-Pro.

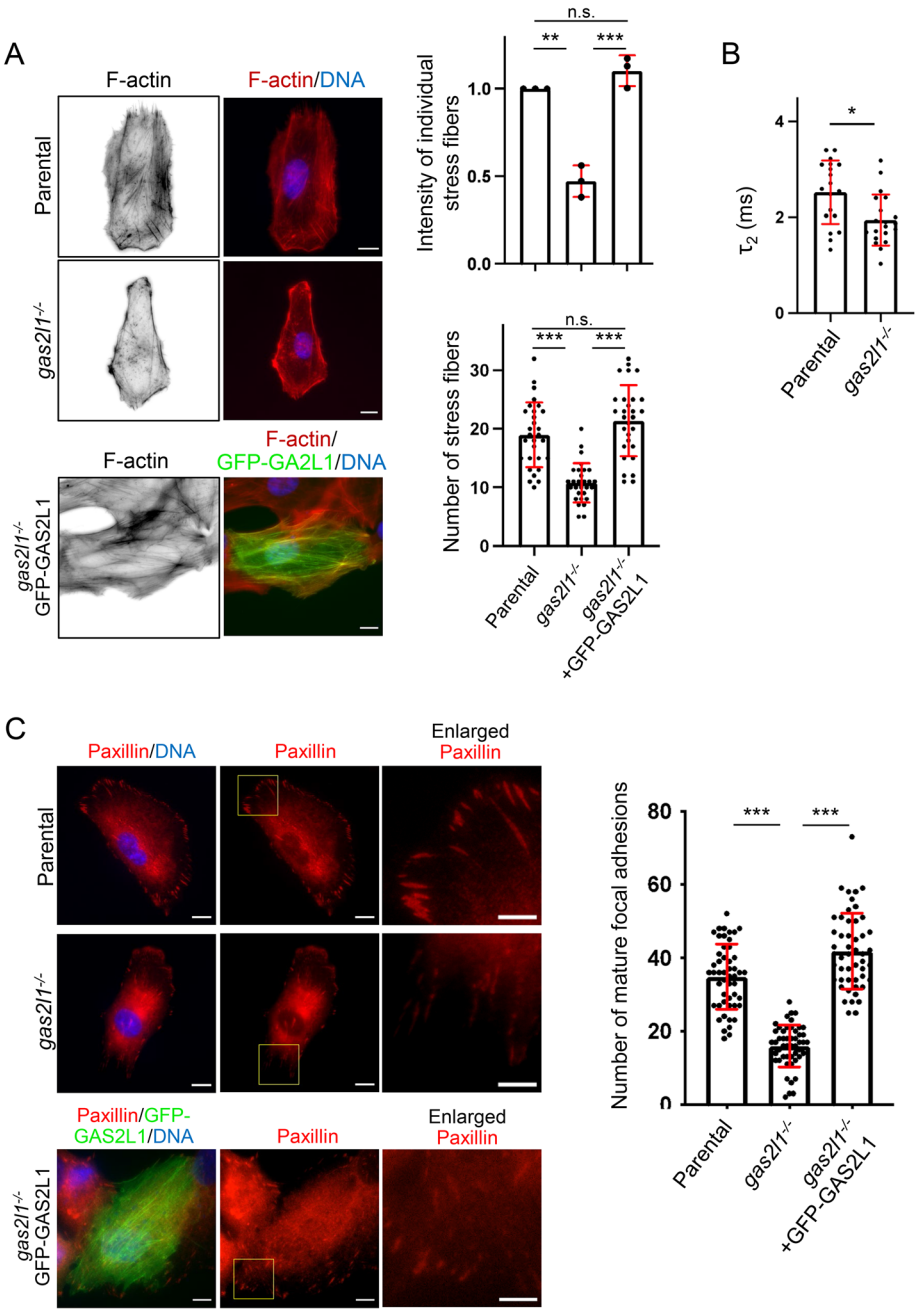

FIGURE 1: GAS2L1 knockout reduces stress fibers and impairs focal adhesions. (A) RPE-1 cells were fixed and stained with phalloidin and Hoechst 33258. Phalloidin-staining intensity of stress fibers was measured from 40 parental cells, 28 *gas2l1*$^{-/-}$ cells and 30 GFP-GAS2L1–expressing *gas2l1*$^{-/-}$ cells. Normalized phalloidin intensities are presented as means ± SD from three independent experiments. The number of actin stress fibers per cell was quantified from 30 cells for each condition across three independent experiments and is shown as mean ± SD. Scale bars, 10 μm. **, $p < 0.001$; ***, $p < 0.0001$; one-way ANOVA test. (B) Mechanical properties of RPE-1 cells were measured using AFM. The shortest response time (τ_2) of the cytoskeleton to indentation was plotted for 19 parental cells and 20 *gas2l1*$^{-/-}$ cells. Data represent mean ± SD from three independent experiments. *, $p < 0.01$; unpaired Student's *t* test. (C) RPE-1 cells were stained for paxillin and nuclear DNA. Mature focal adhesions (defined as paxillin puncta >1 μm^2) were counted in 50 cells for each condition across three independent experiments. Data represent the number of mature focal adhesions per cell (mean ± SD). Scale bars, 10 μm. ***, $p < 0.0001$; one-way ANOVA.

To examine the mechanical properties of the cytoskeleton, we employed atomic force microscopy (AFM)—a technique commonly used to measure cellular stiffness and cytoskeletal dynamics (Hoffman and Crocker, 2009; Moeendarbary and Harris, 2014; Haase and Pelling, 2015; Pegoraro *et al.*, 2017; Guan *et al.*, 2021). We performed cell-indentation tests using a colloidal probe, analyzing force relaxation data to determine the modulus and power-law relaxation parameters of the cytoskeleton. Notably, *gas2l1*$^{-/-}$ cells displayed a ~27% decrease in the power-law relaxation time constant τ_2 (Figure 1B), which represents the time required for the

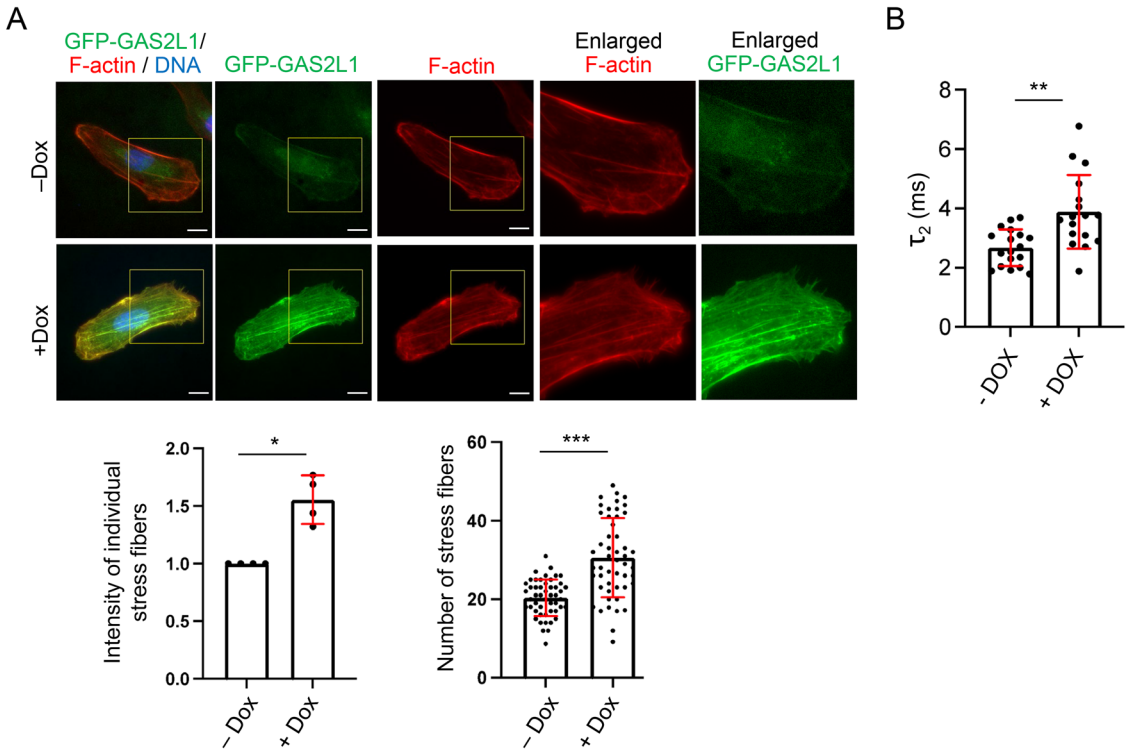

FIGURE 2: GAS2L1 promotes assembly of stress fibers. (A) GFP-GAS2L1 overexpression was induced in *gas2l1*$^{-/-}$ RPE-1 cells by treatment with 1 μg/ml doxycycline (Dox) for 24 h. Control *gas2l1*$^{-/-}$ cells were not treated with Dox. Cells were stained with phalloidin and Hoechst 33258. Phalloidin intensity was quantified from individual stress fibers in 40 control cells and 44 Dox-induced cells across four independent experiments, with data presented as means ± SD The number of actin stress fibers was counted in 50 control cells and 50 Dox-induced cells, and the average number per cell is presented as mean ± SD. *, $p < 0.01$; ***, $p < 0.0001$; unpaired Student's *t* test. Scale bars, 10 μm. (B) AFM was used to measure the shortest response time (τ_2) of the cytoskeleton to indentation in 20 control cells and 17 GFP-GAS2L1–overexpressing cells across three independent experiments. Data are presented as mean ± SD. **, $p < 0.001$; unpaired Student's *t* test.

cytoskeleton to recover after mechanical perturbation (Guan *et al.*, 2021). This suggests that *gas2l1* knockout cells exhibit diminished cytoskeletal resistance to rearrangement upon mechanical stress.

Actin stress fibers play a critical role in the maturation of nascent focal complexes into mature focal adhesions by exerting mechanical forces and serving as a structural template for adhesion growth (Oakes *et al.*, 2012). To investigate the impact of *gas2l1* knockout on focal adhesion dynamics, we stained focal complexes using an antibody against paxillin and classified complexes larger than 1 μm^2 as mature focal adhesions or those undergoing maturation (Kim and Wirtz, 2013; Alday-Parejo *et al.*, 2021). In *gas2l1*$^{-/-}$ cells, the number of mature focal adhesions was reduced by ~49% compared with parental RPE-1 cells, while smaller nascent focal complexes appeared more abundant (Figure 1C). Re-expression of exogenous GAS2L1 rescued the defect in focal adhesion maturation (Figure 1C). These findings indicate that GAS2L1 deficiency disrupts focal adhesion maturation, consistent with the observed reduction in stress fibers. Together, our results demonstrate that GAS2L1 is crucial for the formation and stabilization of stress fibers as well as the maturation of focal adhesions.

To further validate the involvement of GAS2L1 in actin organization, we developed a Tet-On inducible GFP-GAS2L1 expression system in *gas2l1*$^{-/-}$ RPE-1 cells (Au *et al.*, 2020). When expressed at levels comparable to the endogenous protein, GFP-GAS2L1 localized to actin filaments at the cell periphery (Figure 2A), consistent with the distribution of the endogenous protein (data not shown). Upon overexpression, GFP-GAS2L1 was enriched on F-actin structures, including stress fibers, leading to a ~56% increase in the average intensity and a ~50% increase in the number of individual stress fibers (Figure 2A). In addition, the power-law relaxation time constant τ_2, a measure of cytoskeletal resistance, increased by ~46% (Figure 2B). These findings suggest that GAS2L1 promotes stress fiber assembly, thereby enhancing cytoskeletal resistance to mechanical perturbations. In conclusion, our results highlight the essential role of GAS2L1 in actin stress fiber formation and focal adhesion maturation, which together contribute to the structural integrity and mechanical resilience of the cytoskeleton under external forces.

CH domain of GAS2L1 promotes the assembly of stress fibers and focal adhesions

GAS2L1 contains a single CH domain that directly binds to F-actin (Zucman-Rossi *et al.*, 1996; Goriounov *et al.*, 2003; Stroud *et al.*, 2014). To investigate the role of this domain in GAS2L1-mediated actin regulation, we generated two expression constructs: one encoding the CH domain (amino acids 1–196) and another comprising the GAS2L1 region without the CH domain (GAR-Tail, amino acids 197–681) (Figure 3A). Overexpression of the CH domain resulted in a significant increase in the average intensity (~49%) and number (~53%) of individual stress fibers, whereas overexpression of the GAR-Tail construct did not have a noticeable effect on stress

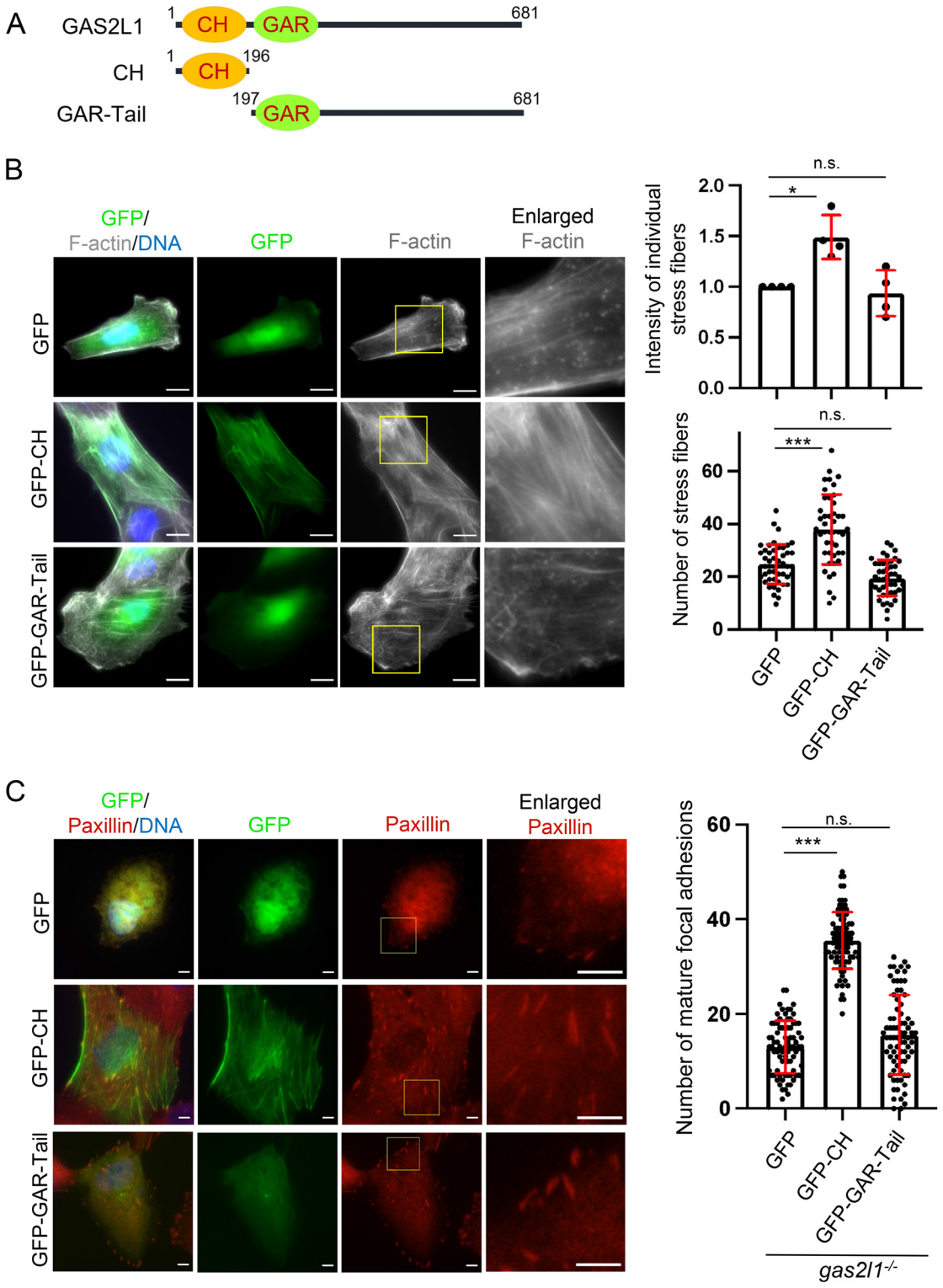

FIGURE 3: CH domain of GAS2L1 promotes formation of stress fibers and focal adhesions. (A) Schematic of GAS2L1 and its fragments. (B) RPE-1 cells expressing GFP, GFP-CH, or GFP-GAR-Tail constructs were stained with phalloidin and Hoechst 33258. Phalloidin intensity of stress fibers was quantified in 35 GFP-expressing cells, 36 GFP-CH–expressing cells, and 32 GFP-GAR-Tail–expressing cells across four independent experiments, with data presented as means ± SD. The average number of actin stress fibers per cell was determined from 45 cells for each condition in four independent experiments and presented as mean ± SD. (C) *gas2l1*$^{-/-}$ RPE-1 cells were transfected with GFP, GFP-CH, or GFP-GAR-Tail constructs and stained with anti-paxillin antibody and Hoechst 33258. Mature focal adhesions (defined as paxillin puncta > 1 μm^2) were quantified in 78 GFP-expressing cells, 90 GFP-CH-expressing cells, and 77 GFP-GAR-Tail-expressing cells across three independent experiments, with data presented as mean ± SD. (B–C) n.s., p>0.01; *, p < 0.01; ***, p < 0.0001; one-way ANOVA. Scale bars, 10 μm.

fiber organization (Figure 3B). These findings demonstrate that the CH domain is responsible for promoting stress fiber assembly.

Next, we assessed whether the CH domain could rescue the focal adhesion defects observed in *gas2l1*$^{-/-}$ RPE-1 cells. Expression of the GAR-Tail construct or the control GFP vector did not restore focal adhesion formation, as indicated by the lack of mature focal adhesions (Figures 3C and 1C). In contrast, expression of the CH domain successfully rescued focal adhesion assembly to levels comparable to those observed in parental RPE-1 cells (Figures 3C and 1C). This rescue effect aligns with the role of the CH domain in promoting stress fiber formation, further supporting the conclusion that GAS2L1's CH domain is crucial for both actin stress fiber assembly and focal adhesion maturation.

CH domain of GAS2L1 induces F-actin bundling and stabilizes F-actin

Stress fibers are bundles of actin filaments cross-linked by various ABPs (Bunai *et al.*, 2006; George *et al.*, 2007; He *et al.*, 2011). To determine whether the single CH domain of GAS2L1 can bundle actin filaments, we performed an in vitro bundling assay. Preassembled actin filaments were incubated either in the absence or presence of the recombinant CH domain of GAS2L1, followed by sedimentation onto coverslips for visualization via microscopy. In the absence of the CH domain, actin filaments appeared randomly distributed, with no evidence of bundling (Figure 4A). In contrast, the addition of the CH domain resulted in the organization of actin filaments into prominent bundles (Figure 4A). As a control, we also tested the GAR domain protein and observed that it did not induce actin bundling (Figure 4A). These results demonstrate that the CH domain of GAS2L1 possesses the ability to bundle F-actin.

Given the ability of the CH domain to bundle actin filaments, we next hypothesized that it might also stabilize F-actin. To test this hypothesis, we preassembled actin filaments using a mixture of pyrene-labeled and unlabeled actin and then incubated the filaments with either the CH domain or a control buffer. F-actin depolymerization was subsequently triggered by diluting the filaments 10-fold into a low-salt buffer containing latrunculin A, an F-actin–depolymerizing agent. Depolymerization of F-actin was monitored by measuring the decrease in pyrene fluorescence. In the absence of the CH domain, the pyrene fluorescence decreased by ∼22% at 1 h postdilution, indicating significant depolymerization (Figure 4B). In contrast, when the CH domain was present, no detectable depolymerization occurred, suggesting that the CH domain prevents F-actin disassembly (Figure 4B).

To further assess the stabilizing effect of the CH domain on actin filaments in a cellular context, we expressed either the CH domain or a GFP control in RPE-1 cells and treated the cells with latrunculin A. Consistent with the in vitro findings, the CH domain expression markedly reduced the depolymerizing effect of latrunculin A: the proportion of cells retaining actin filaments increased from ∼24% in GFP-expressing cells to 81% in cells expressing the CH domain (Figure 4C). This result confirms that the CH domain of GAS2L1 stabilizes actin filaments, both in vitro and in cells.

Dimerization of GAS2L1 CH domain

The formation of actin bundles typically involves the cross-linking of two or more actin filaments, a process that is often facilitated by the dimerization or oligomerization of bound ABPs (Bunai *et al.*, 2006; George *et al.*, 2007; He *et al.*, 2011). Given that the CH domain of GAS2L1 promotes actin bundling, we investigated whether it undergoes dimerization or oligomerization. To test this, we coexpressed two differentially tagged constructs of the GAS2L1 CH domain: one FLAG-tagged and the other GFP-tagged. Immunoprecipitation of the FLAG-tagged CH domain robustly coimmunoprecipitated the GFP-tagged CH domain (Figure 5A, left), indicating that the CH domain engages in intermolecular self-interaction. This coimmunoprecipitation was specific, as GFP-CH was not detected in the anti-FLAG immunoprecipitate when coexpressed with an empty FLAG vector (Figure 5A, left). In addition, the coimmunoprecipitation of GFP-CH by FLAG-CH was unaffected by pretreatment of the cells with the F-actin–depolymerizing agent latrunculin B (Figure 5A, right). These results suggest that the self-interaction of the CH domain is independent of its F-actin–binding activity. In summary, the CH domain of GAS2L1 forms homotypic interactions, which may underlie its ability to promote actin bundling.

Previous studies have shown that the CH and GAR domains of GAS2L1 interact to form an autoinhibitory module (van de Willige *et al.*, 2019; Au *et al.*, 2020). To determine whether the GAR domain modulates CH domain dimerization, we coexpressed the GAR domain with the differentially tagged CH constructs. Remarkably, coexpression of the GAR domain significantly disrupted the coimmunoprecipitation of GFP-CH with FLAG-CH, both in latrunculin B-treated and untreated cells (Figure 5A). Moreover, the GAR protein itself was readily detected in the immunoprecipitate of FLAG-CH (Figure 5A), confirming that the GAR domain binds to the CH domain, thereby interfering with its dimerization.

To further validate the dimerization of the CH domain, we performed chemical cross-linking experiments using the amine-reactive cross-linker bis(sulfosuccinimidyl)suberate (BS^3). After cross-linking, the CH protein was detected as two molecular species: ∼22 kDa, corresponding to the monomeric form, and ∼45 kDa, corresponding to the dimeric form (Figure 5B). Under these cross-linking conditions, ∼22% of the CH protein was present as a dimer (Figure 5B). Conversely, when the CH-GAR protein was subjected to cross-linking under identical conditions, almost all of the protein appeared as a monomer, and the dimeric form was barely detectable (Figure 5B).

Together, these results demonstrate that the CH domain of GAS2L1 forms a dimer through intermolecular self-interaction and that the presence of the GAR domain inhibits this dimerization.

DISCUSSION

In this study, we have characterized the role of GAS2L1 in promoting the assembly of actin stress fibers and the maturation of focal adhesions, and we have elucidated the underlying mechanisms of this function. Our findings indicate that the CH domain of GAS2L1 is responsible for these activities by mediating actin-bundling and stabilizing actin filaments. Specifically, we discovered that the CH domain can dimerize, which facilitates actin filament cross-linking. However, this dimerization is inhibited by the association with the GAR domain, which blocks CH-CH interaction. Given the presence of CH domains in other members of the GAS2 family, it is likely that the functional characteristics observed here for GAS2L1 are conserved across the GAS2 family proteins.

Within the CH domain family, the CH1-CH2 tandem is known as a canonical F-actin–binding module (Gimona *et al.*, 2002; Korenbaum and Rivero, 2002; Yin *et al.*, 2020). Early studies based on mutagenesis and crystal structures supported a closed CH1-CH2 conformation, where the actin-binding surface involves three regions, termed actin-binding sites 1–3 (ABS1–3) (Bresnick *et al.*, 1990; Hemmings *et al.*, 1992; Kuhlman *et al.*, 1992; Levine *et al.*, 1992). More recently, cryo-electron microscopy of the CH1-CH2 complex in association with F-actin revealed that when binding

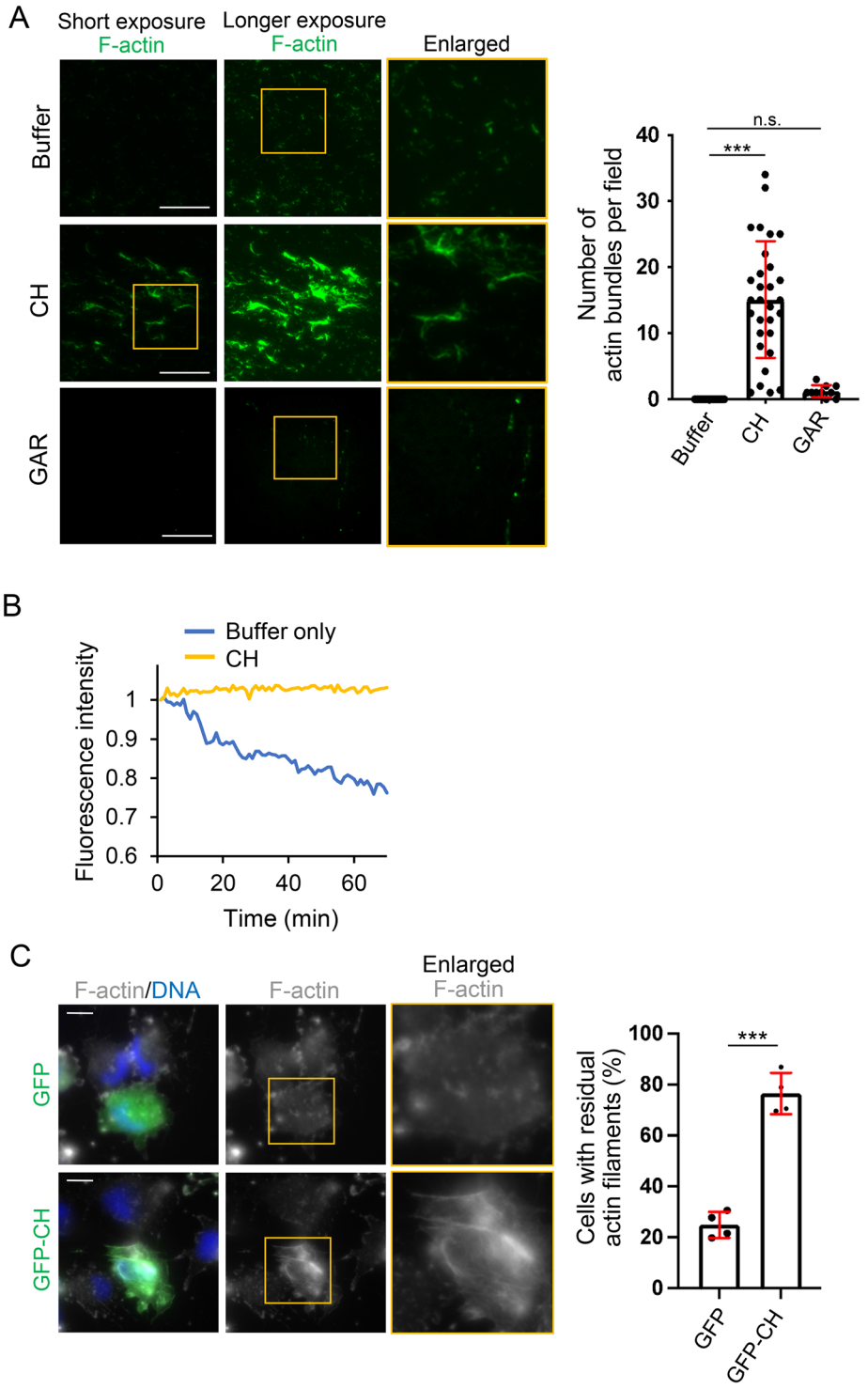

FIGURE 4: CH domain of GAS2L1 induces F-actin bundling. (A) Preassembled F-actin was mixed with recombinant CH protein, GAR protein or buffer and incubated. Proteins were fixed, sedimented onto coverslips by centrifugation, and stained with phalloidin. The average number of bundles per field was measured in three independent experiments and presented as mean ± SD. Each dot represents the number of bundles in an individual field. n.s., $p>0.5$; ***, $p < 0.0001$; one-way ANOVA. Scale bars, 10 μm. (B) F-actin preassembled from a mixture of pyrene-labeled and unlabeled G-actin was incubated with recombinant CH protein or buffer. Pyrene fluorescence was monitored following 10-fold dilution of samples in G-buffer containing latrunculin A to assess F-actin stability. (C) RPE-1 cells transiently expressing GFP-CH or GFP were treated with 1 μM latrunculin A for 30 min and stained with phalloidin and Hoechst 33258. The proportion of cells containing actin filaments was measured in 58 GFP-expressing cells and 67 GFP-CH-expressing cells across three independent experiments (mean ± SD). ***, $p < 0.0001$; unpaired Student's *t* test. Scale bars, 10 μm.

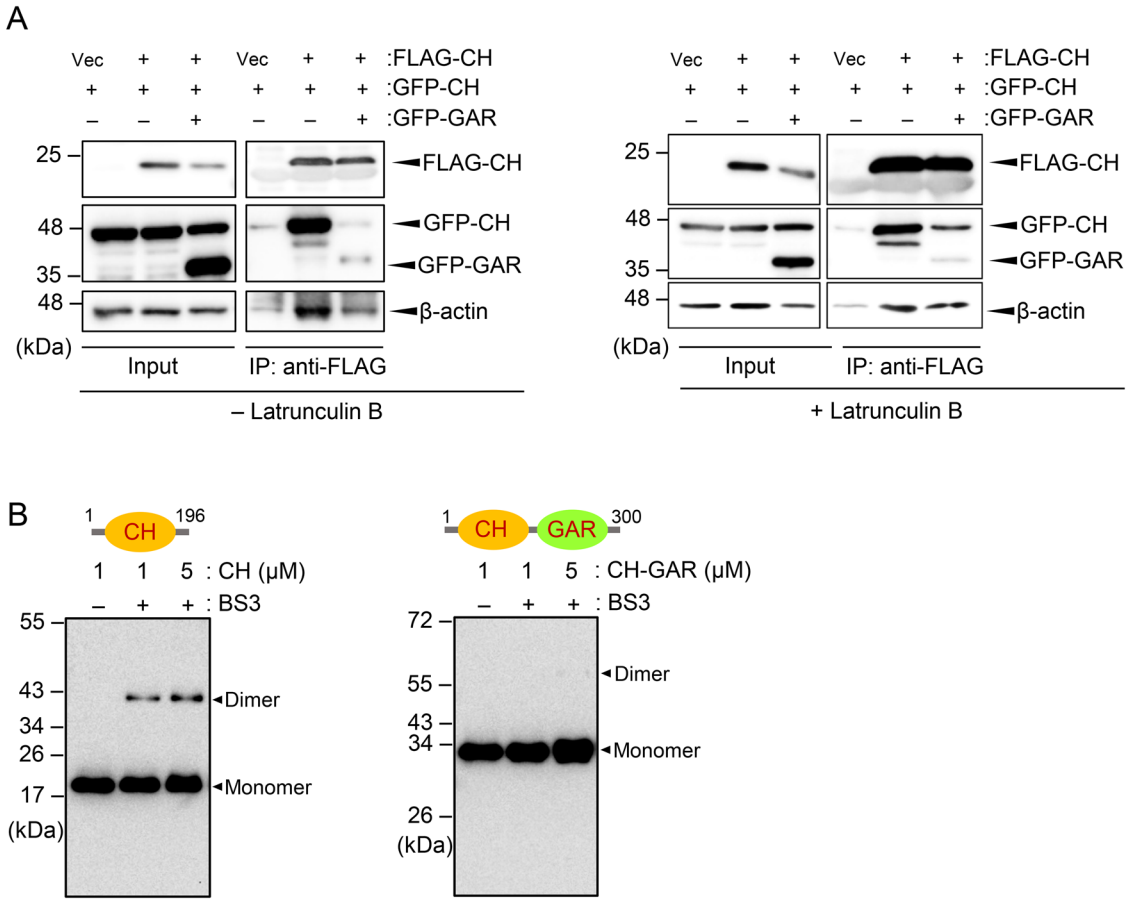

FIGURE 5: Dimerization of GAS2L1 CH domain. (A) FLAG-CH or empty FLAG vector was cotransfected with GFP-CH or GFP-GAR in various combinations. Cells were treated with 1 μM latrunculin B for 1 h (+Latrunculin B) or left untreated (−Latrunculin B) before being subjected to anti-FLAG immunoprecipitation. Immunoprecipitates (50%) and lysate inputs (5%) were analyzed by immunoblotting using anti-FLAG, anti-GFP, and anti-β-actin antibodies. Vec, empty FLAG vector. (B) Recombinant His_6-FLAG-tagged CH and CH-GAR proteins were cross-linked using BS^3. Cross-linked samples were analyzed by anti-His_6 immunoblotting.

to F-actin, CH1 adopts an open conformation with CH2 orientated away from CH1 to expose the actin-binding surface on CH1 (Iwamoto *et al.*, 2018; Kumari *et al.*, 2020). In the closed conformation, CH2 has been suggested to stabilize CH1, thus leading to a soluble structure of CH1-CH2 (Singh *et al.*, 2014; Bandi *et al.*, 2014; Singh *et al.*, 2015).

The CH domain found in GAS2L1 and other GAS2 family proteins belongs to the CH3 subfamily (Gimona *et al.*, 2002; Korenbaum and Rivero, 2002; Goriounov *et al.*, 2003). Because the structure of GAS2L1 has not been experimentally determined, we analyzed its predicted structure using the AlphaFold Protein Structure Database (Figure 6A) (Jumper *et al.*, 2021; Varadi *et al.*, 2022). The predicted structure of the GAS2L1 CH domain was compared to the structure of canonical CH1 domains. Overlaying the predicted structure of GAS2L1 CH with the crystal structure of the spectrin βII CH1 domain, a canonical CH1 domain, revealed that GAS2L1 CH exhibits similar helical orientations, forming a putative actin-binding surface resembling that of CH1 (ABS-N, ABS1, ABS2, and ABS2′; Figure 6, A–C). Interestingly, the GAS2L1 CH domain contains a unique C-terminal helix (Figure 6A, shown in green) absent in spectrin βII CH1 (Figure 6, A and B). This C-terminal helix is distinct from the actin-binding surface formed by other putative ABSs (Figure 6, A and C), despite displaying high sequence similarity to ABS2 of canonical CH1 domains. The functional significance of this unique C-terminal helix remains to be elucidated. Overall, our findings demonstrate that GAS2L1 CH retains structural features of CH1 domains while incorporating unique properties, such as dimerization and actin-bundling activities (Figures 4 and 5). These features likely distinguish GAS2L1 CH from canonical CH1 domains and warrant further investigation.

The CH and GAR domains of GAS2L1 form an autoinhibitory module that regulates their interaction with F-actin and microtubules, respectively (van de Willige *et al.*, 2019; Au *et al.*, 2020). Analysis of the predicted GAS2L1 structure revealed the binding interface between the CH and GAR domains. This interface is located between the microtubule-binding surface of the GAR domain and the C-terminal helix of the CH domain, without significant contact with the putative actin-binding surface formed by ABS-N, ABS1, ABS2, and ABS2′ (Figure 6C). We observed that the GAR domain not only inhibits the interaction of the CH domain with F-actin (Au *et al.*, 2020) but also suppresses CH domain dimerization (Figure 5). It is likely that the C-terminal helix of GAS2L1 CH plays a role in dimerization, a process inhibited by its interaction with the GAR domain. In addition, the expression of GAS2L1 CH alone resulted in low solubility, whereas the CH-GAR construct demonstrated enhanced solubility (data not shown). This suggests that the

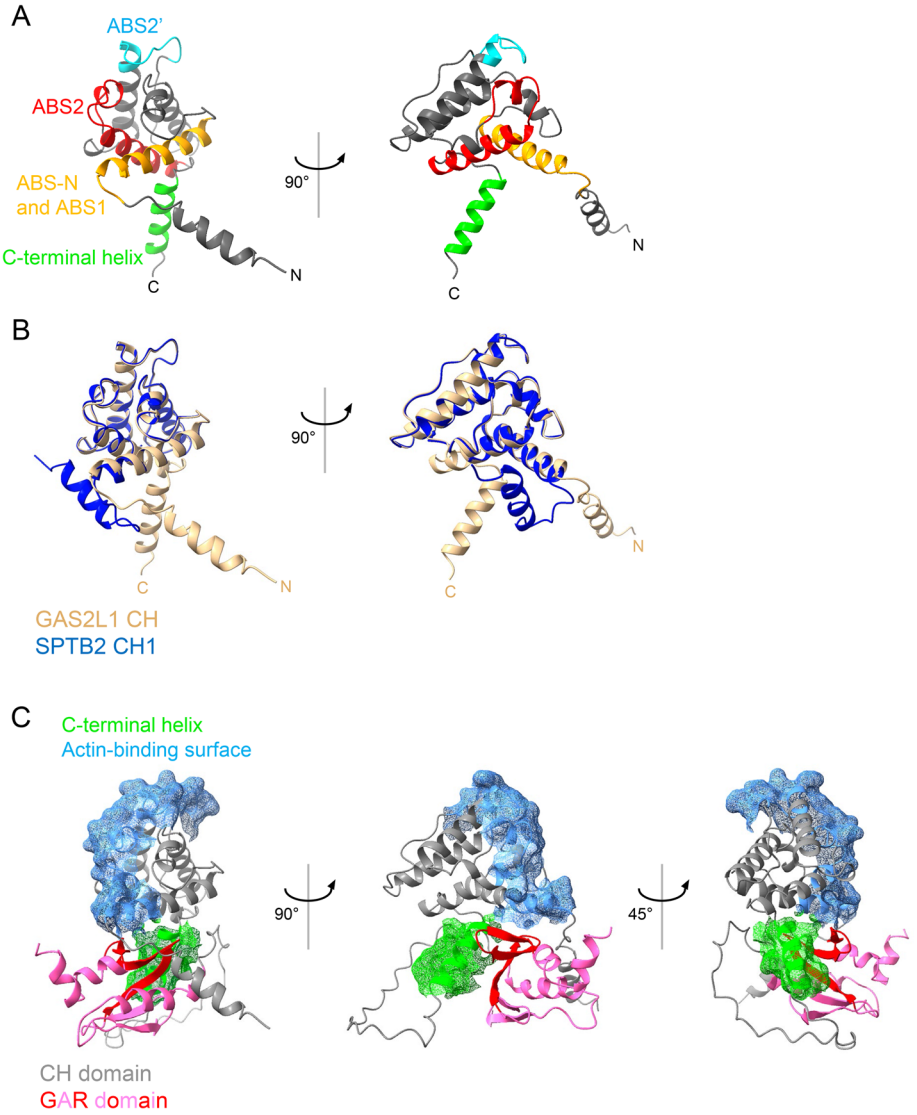

FIGURE 6: Modeling the structure of CH and GAR domains. (A) AlphaFold structural model of the GAS2L1 CH domain (residues 1–171). Putative actin-binding sites (ABS-N and ABS1) are indicated in orange, ABS2 in red, and ABS2′ in cyan. The C-terminal helix is highlighted in green. (B) Overlay of the AlphaFold structure of the GAS2L1 CH domain (beige) with the crystal structure of spectrin βII CH1 domain (blue; PDB identifier: 1BKR), represented as ribbon diagrams. (C) Structural model of the CH-GAR module (residues 1–281) generated by AlphaFold. The CH domain is depicted in gray, and the GAR domain in pink and red. The actin-binding interface of the CH domain is shown in light blue, while its C-terminal helix is highlighted in green. The microtubule-binding surface of the GAR domain (red) is closely associated with the C-terminal helix of the CH domain.

GAR domain may stabilize the CH domain, similar to how CH2 stabilizes CH1 in the CH1-CH2 tandem. The autoinhibition of the CH-GAR module in GAS2L1 is relieved by phosphorylation at Ser352 by Nek2 during late G2 and mitosis (Au *et al.*, 2020). This mechanism suggests that GAS2L1 may play a role in actin reorganization as cells enter mitosis.

Actin stress fibers are bundles of actin filaments cross-linked by proteins such as α-actinin, which are crucial for maintaining cell shape and facilitating cell movement (Naumanen *et al.*, 2008; Tojkander *et al.*, 2012). Based on their orientation and association with focal adhesions, stress fibers can be classified as dorsal stress fibers, ventral stress fibers, or transverse arcs (Naumanen *et al.*, 2008; Tojkander *et al.*, 2012). A number of actin-cross-linking proteins, including β-spectrin, paladin, fascin, filamin, and α-actinin, have been identified as stabilizers of stress fibers (Naumanen *et al.*, 2008; Tojkander *et al.*, 2012). In this study, we show that GAS2L1 promotes stress fiber assembly through its CH domain, which possesses actin-bundling and stabilizing activities. Consistently, knockout of *gas2l1* impaired the formation of stress fibers (Figure 1A). A recent study highlighted the role of actin-microtubule cross-linkers that track microtubule plus ends in facilitating the transport of actin filaments by growing microtubules (Alkemade *et al.*, 2022). Because GAS2L1 has been shown to track microtubule plus ends (Jiang *et al.*, 2012; Stroud *et al.*, 2014), it is likely that GAS2L1 contributes to stress fiber remodeling through microtubule-mediated actin filament transport. Given these unique properties, GAS2L1

may play a distinctive role compared to other ABPs in the formation and regulation of stress fibers.

Actin stress fibers are crucial for the assembly of focal adhesions, which are sites of integrin-mediated cell adhesion to the extracellular matrix (Chrzanowska-Wodnicka and Burridge, 1996; Riveline *et al.*, 2001; Zaidel-Bar *et al.*, 2003; Peterson *et al.*, 2004; Vicente-Manzanares *et al.*, 2007; Choi *et al.*, 2008; Oakes *et al.*, 2012). By contrast, microtubules target focal adhesions for disassembly (Kaverina *et al.*, 1998, 1999; Etienne-Manneville, 2013). GAS2L1 interacts with both F-actin and microtubules, associating with microtubules and microtubule plus ends through the GAR domain and the SxIP motif in its tail region, respectively (Goriounov *et al.*, 2003; Jiang *et al.*, 2012; Stroud *et al.*, 2014). Our study demonstrates that the CH domain of GAS2L1 promotes stress fiber and focal adhesion formation, independent of the GAR domain or tail region (Figure 3). However, the microtubule-binding and plus-end-tracking properties may play a role in guiding microtubules to focal adhesions. This suggests that GAS2L1 has a multifaceted role in regulating focal adhesion dynamics.

MATERIALS AND METHODS

Request a protocol through *Bio-protocol*

Antibodies

The following primary antibodies were obtained from commercial sources: mouse anti-paxillin (Clone 349, BD Biosciences), mouse anti-FLAG (Clone M2, Sigma-Aldrich), and rabbit anti-FLAG (Sigma-Aldrich). The antibody against GFP was custom-generated and utilized as described previously (Au *et al.*, 2017).

Cell culture and treatments

All cell lines used in this study were sourced from the American Type Culture Collection. HEK293T cells were maintained in DMEM (Gibco) supplemented with 10% FBS and 100 U/ml penicillin/streptomycin mix. RPE-1 cells were cultured in a 1:1 mixture of DMEM and Ham's F12 medium containing 10% FBS, 100 U/ml penicillin-streptomycin, and 10 µg/ml hygromycin B (Sigma-Aldrich). *gas2l1* knockout RPE-1 cells (*gas2l1*$^{-/-}$) were generated as previously described; *gas2l1*$^{-/-}$ lines harboring an inducible expression cassette of GFP-GAS2L1 were created using a tet-on expression system, with GFP-GAS2L1 expression induced for 24 h by adding 1 µg/ml doxycycline (Sigma-Aldrich) to the culture medium (Au *et al.*, 2020). Transient transfection of RPE-1 and HEK293T cells was performed using Lipofectamine 2000 (Thermo Fisher Scientific) and polyethylenimine (Polysciences), respectively. All cells were maintained in a humidified incubator at 37°C with 5% CO_2 and were routinely tested to ensure they were free of Mycoplasma contamination.

Immunofluorescence microscopy

Cells grown on 18-mm coverslips were fixed with 4% paraformaldehyde in PBS for 15 min at room temperature, then washed twice with PBS. After blocking with 2% BSA in PBS containing 0.05% Tween 20, the cells were stained sequentially at room temperature using a primary antibody followed by an Alexa Fluor 568-conjugated secondary antibody (Thermo Fisher Scientific). Nuclear DNA was stained with 1 µM Hoechst 33258 (Sigma-Aldrich), and F-actin was labeled with Alexa Fluor 647-conjugated phalloidin (Thermo Fisher Scientific). Fluorescence images were captured using an epifluorescence microscope (Axio Observer ZI; Carl Zeiss) equipped with a DAPI/GFP/Texas-Red/Cy5 filter set, an X-Cite 120Q light source (Lumen Dynamics), and an sCMOS camera (Orca-Flash4.0, Hamamatsu). Images were analyzed and processed using ZEN 3.0 software (blue edition, Carl Zeiss) and the Fiji package of ImageJ (Schindelin *et al.*, 2012).

Actin stress fibers were manually identified within each cell, and the phalloidin-staining intensity of individual fibers was quantified using the Line Selection tool in the Fiji package of ImageJ (Schindelin *et al.*, 2012). To account for background fluorescence, signals were also measured in adjacent cytoplasmic regions devoid of visible actin filaments. Paxillin puncta were detected using a predefined threshold in the Analyze Particles tool within Fiji (Schindelin *et al.*, 2012). Puncta larger than 1 µm^2 were classified as mature focal adhesions and subsequently counted.

Atomic force microscopy

To assess the cytoskeletal mechanics of RPE-1 cells, we utilized an atomic force microscope (MFP-3D, Asylum Research) equipped with a spherical probe for cell indentation. The spherical probes were prepared according to an established protocol by attaching a glass bead (diameter ~12 µm) to the front end of a tipless cantilever (CSC38/Tipless/Cr-Au, Mikromasch) with a nominal spring constant of ~0.09 N/m (Guan *et al.*, 2021). To ensure precise force measurements, the spring constant of each cantilever was calibrated using the power density spectrum method (Guan *et al.*, 2021). Prior to experimentation, the colloidal probes were coated with a thin layer of poly(L-lysine)-graft-poly(ethylene glycol) (SuSoS AG) to minimize adhesion between the cell surface and the probe.

During the AFM measurements, RPE-1 cells cultured on a coverslip were maintained in a growth medium at 37°C in a humidified chamber with 5% CO_2. The spherical probe was rapidly approached to the cell surface and held in close contact for 10 s, inducing a constant indentation. Subsequently, the force relaxation, defined as the force dissipation over time (t), was recorded to capture the cell's mechanical response to external compression. Analysis of the relaxation data revealed that the mechanical properties of the cells could be described by the relaxation modulus, $E(t) = E_1\, e^{-t/\tau_1} + E_2(1 + t/\tau_2)^{-\alpha} + E_\infty$. Here, E_1, E_2, and E_∞ correspond to the exponential, power-law, and persistent moduli, respectively; τ_1 and τ_2 represent the timescales for exponential and power-law decays, and α is the power-law exponent (Guan *et al.*, 2021). Among these components, the power-law relaxation time, determined by τ_2, is indicative of cytoskeletal network reorganization under compression.

F-actin-bundling and stabilization assays

GAS2L1 fragments (CH, 1–196; GAR, 197–300; CH-GAR 1–300) tagged with His_6-FLAG were expressed in *Escherichia coli* BL21 (DE3) and purified using Ni^{2+}-nitrilotriacetic acid resin (Qiagen), as described previously (Au *et al.*, 2020). Before use in assays, the proteins were desalted and diluted in actin polymerization buffer (10 mM Tris-HCl, pH 7.5, 50 mM KCl, 2 mM $MgCl_2$, 1 mM ATP).

For the bundling assay, F-actin was polymerized by incubating 10 µM preclarified rabbit skeletal muscle G-actin (99% purity; Cytoskeleton Inc.) in actin polymerization buffer for 1 h at room temperature. After assembly, an equal volume of actin polymerization buffer containing 10 µM GAS2L1 proteins was added, and the mixture was incubated for an additional 30 min. F-actin filaments and bundles were then fixed for 5 min with 1% glutaraldehyde in polymerization buffer and pelleted onto coverslips through a glycerol cushion (10% glycerol in actin polymerization buffer) by centrifugation at 100,000 × g for 10 min at 24°C. The filaments and bundles were stained with Alexa Fluor 647-conjugated phalloidin (Thermo Fisher Scientific) and visualized using a fluorescence microscope.

The F-actin stabilization assay was conducted as previously described, with modifications (He *et al.*, 2011). F-actin was polymerized using 4 μM preclarified rabbit skeletal muscle G-actin (5% pyrene-labeled; Cytoskeleton Inc.) and pelleted through a glycerol cushion by centrifugation at 150,000 × *g* for 30 min at 24°C. The pellets were resuspended in actin polymerization buffer containing GAS2L1 proteins, incubated at room temperature for 15 min, and then diluted 10-fold in G-buffer (5 mM Tris-HCl, pH 8.0, 0.2 mM $CaCl_2$) containing 1 μM latrunculin A. F-actin depolymerization was monitored by measuring pyrene fluorescence using a microplate reader (FlexStation 3, Molecular Devices).

Immunoprecipitation

HEK293T cells expressing FLAG-tagged GAS2L1 proteins were lysed in buffer containing 50 mM HEPES (pH 7.4), 0.5% Triton X-100, 150 mM NaCl, 1 mM $MgCl_2$, 10 mM NaF, 1 mM dithiothreitol, and a Protease Inhibitor Cocktail (Bimake). The lysates were clarified by centrifugation at 16,000 × *g* for 15 min at 4°C. Immunoprecipitation was performed at 4°C for 2 h with rotation using anti-FLAG M2 affinity agarose beads (Sigma-Aldrich). The beads were then washed extensively with buffer containing 50 mM HEPES (pH 7.4), 0.1% Triton X-100, 150 mM NaCl, 1 mM $MgCl_2$, and 1 mM dithiothreitol, followed by boiling at 95°C to elute proteins for SDS–PAGE and immunoblotting.

Chemical cross-linking

Recombinant GAS2L1 proteins were cross-linked on ice for 2 h using BS^3 (Thermo Fisher Scientific) at a 50-fold molar excess. The reactions were quenched by adding 1 M Tris-HCl (pH 7.5) to a final concentration of 50 mM, and the cross-linked proteins were subsequently analyzed by immunoblotting.

Statistical analysis

All quantitative data were derived from at least three independent experiments. Statistical analyses were performed using MATLAB, Microsoft Excel, or GraphPad Prism, with specific tests outlined in the figure legends. For comparisons between two samples, *p*-values were calculated using an unpaired Student's *t* test. For comparisons involving more than two conditions, one-way ANOVA followed by Tukey's test was used to determine statistically significant differences between samples.

ACKNOWLEDGMENTS

We sincerely thank Dr. Anna Akhmanova (Utrecht University, The Netherlands) for her critical review and valuable feedback on the manuscript. This work was supported by grants from the Research Grants Council (General Research Fund 16100820 and 16300421 and Theme-based Research Scheme T13-605/18-W) and the Innovation and Technology Commission (ITCPD/17-9) of Hong Kong, HKUST Aging Research Grant (Z1056), Shenzhen Science and Technology Committee Research Grant (SGDX20210823103200005), Guangdong Provincial Key Lab of Integrated Communication (Sensing and Computation for Ubiquitous Internet of Things [No. 2023B1212010007]), and Guangzhou Science and Technology Program City-University Joint Funding Project (2023A03J0001). F.K.C.A. was supported by the Postdoctoral Fellowship Scheme (PDFS2021-6S03), and K.T.D.L was supported by the Hong Kong PhD Fellowship Scheme (PF21-60517) from the Research Grants Council of Hong Kong.

REFERENCES

Alday-Parejo B, Ghimire K, Coquoz O, Albisetti GW, Tamò L, Zaric J, Stalin J, Rüegg C (2021). MAGI1 localizes to mature focal adhesion and modulates endothelial cell adhesion, migration and angiogenesis. Cell Adhes Migr 15, 126–139.

Alkemade C, Wierenga H, Volkov VA, Preciado López M, Akhmanova A, ten Wolde PR, Dogterom M, Koenderink, GH (2022). Cross-linkers at growing microtubule ends generate forces that drive actin transport. Proc Natl Acad Sci U S A 119, e2112799119.

Au FKC, Hau BKT, Qi RZ (2020). Nek2-mediated GAS2L1 phosphorylation and centrosome-linker disassembly induce centrosome disjunction. J Cell Biol 219, e201909094.

Au FKC, Jia Y, Jiang K, Grigoriev I, Hau BKT, Shen Y, Du S, Akhmanova A, Qi RZ (2017). GAS2L1 is a centriole-associated protein required for centrosome dynamics and disjunction. Dev Cell 40, 81–94.

Bandi S, Singh SM, Mallela KMG (2014). The C-terminal domain of the utrophin tandem calponin-homology domain appears to be thermodynamically and kinetically more stable than the full-length protein. Biochemistry 53, 2209–2211.

Bañuelos S, Saraste M, Carugo KD (1998). Structural comparisons of calponin homology domains: implications for actin binding. Structure 6, 1419–1431.

Bresnick AR, Warren V, Condeelis J (1990). Identification of a short sequence essential for actin binding by Dictyostelium ABP-120. J Biol Chem 265, 9236–9240.

Bunai F, Ando K, Ueno H, Numata O (2006). Tetrahymena eukaryotic translation elongation factor 1A (eEF1A) bundles filamentous actin through dimer formation. J Biochem (Tokyo) 140, 393–399.

Carlsson AE (2010). Actin dynamics: From nanoscale to microscale. Annu Rev Biophys 39, 91–110.

Choi CK, Vicente-Manzanares M, Zareno J, Whitmore LA, Mogilner A, Horwitz AR (2008). Actin and α-actinin orchestrate the assembly and maturation of nascent adhesions in a myosin II motor-independent manner. Nat Cell Biol 10, 1039–1050.

Chrzanowska-Wodnicka M, Burridge K (1996). Rho-stimulated contractility drives the formation of stress fibers and focal adhesions. J Cell Biol 133, 1403–1415.

dos Remedios CG, Chhabra D, Kekic M, Dedova IV, Tsubakihara M, Berry DA, Nosworthy NJ (2003). Actin binding proteins: Regulation of cytoskeletal microfilaments. Physiol Rev 83, 433–473.

Etienne-Manneville S (2013). Microtubules in cell migration. Annu Rev Cell Dev Biol 29, 471–499.

Gamper I, Fleck D, Barlin M, Spehr M, El Sayad S, Kleine H, Maxeiner S, Schalla C, Aydin G, Hoss M, *et al.* (2016). GAR22β regulates cell migration, sperm motility, and axoneme structure. Mol Biol Cell 27, 277–294.

Gardel ML, Schneider IC, Aratyn-Schaus Y, Waterman CM (2010). Mechanical integration of actin and adhesion dynamics in cell migration. Annu Rev Cell Dev Biol 26, 315–333.

Geiger B, Yamada KM (2011). Molecular architecture and function of matrix adhesions. Cold Spring Harb Perspect Biol 3, a005033.

George SP, Wang Y, Mathew S, Srinivasan K, Khurana S (2007). Dimerization and actin-bundling properties of villin and its role in the assembly of epithelial cell brush borders. J Biol Chem 282, 26528–26541.

Gimona M, Djinovic-Carugo K, Kranewitter WJ, Winder SJ (2002). Functional plasticity of CH domains. FEBS Lett 513, 98–106.

Goriounov D, Leung CL, Liem RKH (2003). Protein products of human Gas2-related genes on chromosomes 17 and 22 (hGAR17 and hGAR22) associate with both microfilaments and microtubules. J Cell Sci 116, 1045–1058.

Guan D, Shen Y, Zhang R, Huang P, Lai P-Y, Tong P (2021). Unified description of compressive modulus revealing multiscale mechanics of living cells. Phys Rev Res 3, 043166.

Haase K, Pelling AE (2015). Investigating cell mechanics with atomic force microscopy. J R Soc Interface 12, 20140970.

He L, Zhang Z, Yu Y, Ahmed S, Cheung NS, Qi RZ (2011). The neuronal p35 activator of Cdk5 is a novel F-actin binding and bundling protein. Cell Mol Life Sci 68, 1633–1643.

Hemmings L, Kuhlman PA, Critchley DR (1992). Analysis of the actin-binding domain of alpha-actinin by mutagenesis and demonstration that dystrophin contains a functionally homologous domain. J Cell Biol 116, 1369–1380.

Hoffman BD, Crocker JC (2009). Cell mechanics: Dissecting the physical responses of cells to force. Annu Rev Biomed Eng 11, 259–288.

Hotulainen P, Lappalainen P (2006). Stress fibers are generated by two distinct actin assembly mechanisms in motile cells. J Cell Biol 173, 383–394.

Iwamoto DV, Huehn A, Simon B, Huet-Calderwood C, Baldassarre M, Sindelar CV, Calderwood DA (2018). Structural basis of the filamin A actin-binding domain interaction with F-actin. Nat Struct Mol Biol 25, 918–927.

Jiang K, Toedt G, Montenegro Gouveia S, Davey NE, Hua S, van der Vaart B, Grigoriev I, Larsen J, Pedersen LB, Bezstarosti K, *et al.* (2012). A proteome-wide screen for mammalian SxIP motif-containing microtubule plus-end tracking proteins. Curr Biol 22, 1800–1807.

Jumper J, Evans R, Pritzel A, Green T, Figurnov M, Ronneberger O, Tunyasuvunakool K, Bates R, Žídek A, Potapenko A, *et al*. (2021). Highly accurate protein structure prediction with AlphaFold. Nature 596, 583–589.

Kadzik RS, Homa KE, Kovar DR (2020). F-actin cytoskeleton network self-organization through competition and cooperation. Annu Rev Cell Dev Biol 36, 35–60.

Kaverina I, Krylyshkina O, Small JV (1999). Microtubule targeting of substrate contacts promotes their relaxation and dissociation. J Cell Biol 146, 1033–1044.

Kaverina I, Rottner K, Small JV (1998). Targeting, capture, and stabilization of microtubules at early focal adhesions. J Cell Biol 142, 181–190.

Kim D-H, Wirtz D (2013). Focal adhesion size uniquely predicts cell migration. FASEB J 27, 1351–1361.

Korenbaum E, Rivero F (2002). Calponin homology domains at a glance. J Cell Sci 115, 3543–3545.

Kuhlman PA, Hemmings L, Critchley DR (1992). The identification and characterisation of an actin-binding site in α-actinin by mutagenesis. FEBS Lett 304, 201–206.

Kumari A, Kesarwani S, Javoor MG, Vinothkumar KR, Sirajuddin M (2020). Structural insights into actin filament recognition by commonly used cellular actin markers. EMBO J 39, e104006.

Levine BA, Moir AJ, Patchell VB, Perry SV (1992). Binding sites involved in the interaction of actin with the N-terminal region of dystrophin. FEBS Lett 298, 44–48.

Moeendarbary E, Harris AR (2014). Cell mechanics: Principles, practices, and prospects. Wiley Interdiscip Rev Syst Biol Med 6, 371–388.

Naumanen P, Lappalainen P, Hotulainen P (2008). Mechanisms of actin stress fibre assembly. J Microsc 231, 446–454.

Oakes PW, Beckham Y, Stricker J, Gardel ML (2012). Tension is required but not sufficient for focal adhesion maturation without a stress fiber template. J Cell Biol 196, 363–374.

Parsons JT, Horwitz AR, Schwartz MA (2010). Cell adhesion: Integrating cytoskeletal dynamics and cellular tension. Nat Rev Mol Cell Biol 11, 633–643.

Pegoraro AF, Janmey P, Weitz DA (2017). Mechanical properties of the cytoskeleton and cells. Cold Spring Harb Perspect Biol 9, a022038.

Peterson LJ, Rajfur Z, Maddox AS, Freel CD, Chen Y, Edlund M, Otey C, Burridge K (2004). Simultaneous stretching and contraction of stress fibers in vivo. Mol Biol Cell 15, 3497–3508.

Pollard TD, Cooper JA (1986). Actin and actin-binding proteins. A critical evaluation of mechanisms and functions. Annu Rev Biochem 55, 987–1035.

Riveline D, Zamir E, Balaban NQ, Schwarz US, Ishizaki T, Narumiya S, Kam Z, Geiger B, Bershadsky AD (2001). Focal contacts as mechanosensors: externally applied local mechanical force induces growth of focal contacts by an mDia1-dependent and ROCK-independent mechanism. J Cell Biol 153, 1175–1186.

Schindelin J, Arganda-Carreras I, Frise E, Kaynig V, Longair M, Pietzsch T, Preibisch S, Rueden C, Saalfeld S, Schmid B, *et al.* (2012). Fiji: An open-source platform for biological-image analysis. Nat Methods 9, 676–682.

Schneider C, King RM, Philipson L (1988). Genes specifically expressed at growth arrest of mammalian cells. Cell 54, 787–793.

Singh SM, Bandi S, Mallela KMG (2015). The N- and C-terminal domains differentially contribute to the structure and function of dystrophin and utrophin tandem calponin-homology domains. Biochemistry 54, 6942–6950.

Singh SM, Bandi S, Winder SJ, Mallela KMG (2014). The actin binding affinity of the utrophin tandem calponin-homology domain is primarily determined by its N-terminal domain. Biochemistry 53, 1801–1809.

Skau CT, Waterman CM (2015). Specification of architecture and function of actin structures by actin nucleation factors. Annu Rev Biophys 44, 285–310.

Stroud MJ, Kammerer RA, Ballestrem C (2011). Characterization of G2L3 (GAS2-like 3), a new microtubule- and actin-binding protein related to spectraplakins. J Biol Chem 286, 24987–24995.

Stroud MJ, Nazgiewicz A, McKenzie EA, Wang Y, Kammerer RA, Ballestrem C (2014). GAS2-like proteins mediate communication between microtubules and actin through interactions with end-binding proteins. J Cell Sci 127, 2672–2682.

Tojkander S, Gateva G, Lappalainen P (2012). Actin stress fibers – assembly, dynamics and biological roles. J Cell Sci 125, 1855–1864.

Varadi M, Anyango S, Deshpande M, Nair S, Natassia C, Yordanova G, Yuan D, Stroe O, Wood G, Laydon A, *et al.* (2022). AlphaFold protein structure database: Massively expanding the structural coverage of protein-sequence space with high-accuracy models. Nucleic Acids Res 50, D439–D444.

Vicente-Manzanares M, Zareno J, Whitmore L, Choi CK, Horwitz AF (2007). Regulation of protrusion, adhesion dynamics, and polarity by myosins IIA and IIB in migrating cells. J Cell Biol 176, 573–580.

van de Willige D, Hummel JJ, Alkemade C, Kahn OI, Au FK, Qi RZ, Dogterom M, Koenderink GH, Hoogenraad CC, Akhmanova A (2019). Cytolinker Gas2L1 regulates axon morphology through microtubule-modulated actin stabilization. EMBO Rep 20, e47732.

Yin L-M, Schnoor M, Jun C-D (2020). Structural characteristics, binding partners and related diseases of the calponin homology (CH) domain. Front Cell Dev Biol 8, 342.

Zaidel-Bar R, Ballestrem C, Kam Z, Geiger B (2003). Early molecular events in the assembly of matrix adhesions at the leading edge of migrating cells. J Cell Sci 116, 4605–4613.

Zucman-Rossi J, Legoix P, Thomas G (1996). Identification of new members of the Gas2 and Ras families in the 22q12 chromosome region. Genomics 38, 247–254.